Analog Feedback Controller for MEMS Microphone

Design Group 32

Wesley Chiu, EE
Andrew Steinmann, EE
Adam Hess, EE

Faculty Advisor: Ron Miles, Eva Wu
Sponsor: Binghamton University

December 11, 2009

Submitted in partial fulfillment of the requirements of ME 493/EECE 487 in the Fall Semester of 2009.

Thomas J. Watson School of Engineering and Applied Science
State University of New York at Binghamton

Abstract

Currently a MicroElectroMechanical System(MEMS) microphone is being developed for next generation hearing aid applications. The microphone is modeled after the ears of the *Ormia ochracea* fly which will allow a micro-scale microphone to not only detect sound pressure, but the direction which the sound is coming from as well. Although the very small size is desirable to reduce thermal noise, it significantly reduces the damping ratio which causes an undesirable resonant peak. The resonant peak creates a ringing noise that is unacceptable for a hearing aid application. In order to eliminate the resonant peak, feedback will be added to adjust the closed loop system poles to remove the resonance and shape the closed loop frequency response. This paper describes the design process used to develop and implement the proper feedback controller as well as potential problems in the feedback design. An initial feedback controller is proposed and analyzed using Matlab and PSpice. Matlab simulations are performed to confirm the validity of the design and PSpice simulations are used to test the analog circuit realization of the controller. The controller has been prototyped on a breadboard and will be tested using the laser vibrometer sensing mechanism.

Table of Contents

List of Figures

I. Introduction

The MEMS microphone currently being developed has some clear advantages over the current generations of hearing aids. The *Ormia ochracea* fly has the unique ability to sense the direction of sound as well as the sound itself. Using the fly's sound sensing capability as motivation, a MEMS microphone was mechanically modeled after the ears. Figure 1 show the mechanical interpretation of the *Ormia ochracea* ears, [1]. The microphone rotates around a pivot point in response to sound excitation. One major improvement of the MEMS microphone over current hearing aid microphones is the significantly lower noise floor. The lower noise floor not only allows the user to hear quieter sounds, but also reduces the magnitude of electronic noise. Another improvement of the MEMs microphone is its directional sensing aspect. Current hearing aids have poor performance in noisy environments because the hearing aids amplify all the surrounding noise. The MEMs microphone is capable of detecting what direction noise is coming from and may reduce background noise and allow the user to focus on what they would like to hear. For example, if the user is sitting in a noisy restaurant the MEMS microphone may be able to reduce the background noise and enable the user to more easily carry a conversation with the person across the table.

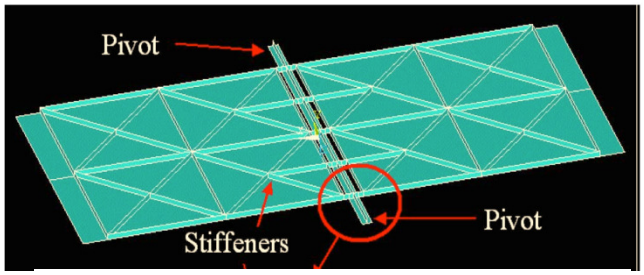

Figure 1 : Microphone

One problem encountered in the development process is creating a small device that does not have a large resonance. One way to decrease the resonance would to increase the stiffness but that would result in a larger device. The larger device may remove the resonant peak, but the size required to do that may be significantly larger. In addition to the size trade off, the device's thermal noise is related to the size. Therefore by increasing the size significantly, there is a significant increase in noise. Since one of the desirable traits of the microphone is the lower noise floor, this option is not ideal. Another option is to introduce a feedback controller to change the transfer function of the system and thereby eliminating the resonant peak. The feedback controller adds additional circuitry to the microphone which is an additional source of noise. However, carefully chosen parts can minimize how much the device raises the noise floor, thereby making a feedback controller the optimal solution.

Figure 2 is the overall block diagram of the microphone and feedback controller. A proportional-derivative controller is chosen to allow flexibility when selecting the desired closed loop system poles. The PD controller's gains have been calculated to a set value, but will be left variable for increased flexibility. The bias voltage as well as the proportional and derivative signals are added together using a summing circuit. The summing circuit outputs the control effort which is then applied to the microphone. In addition to the PD controller circuit, there is also an audio amplifier circuit which will allow the user to hear the outputted sound via headphones. The PD controller circuit and audio amplifier will be powered using two 9 volt batteries to provide positive and negative voltage rails required by the op-amps. The controller and audio circuit will be enclosed in a metal chassis to reduce electromagnetic interference and

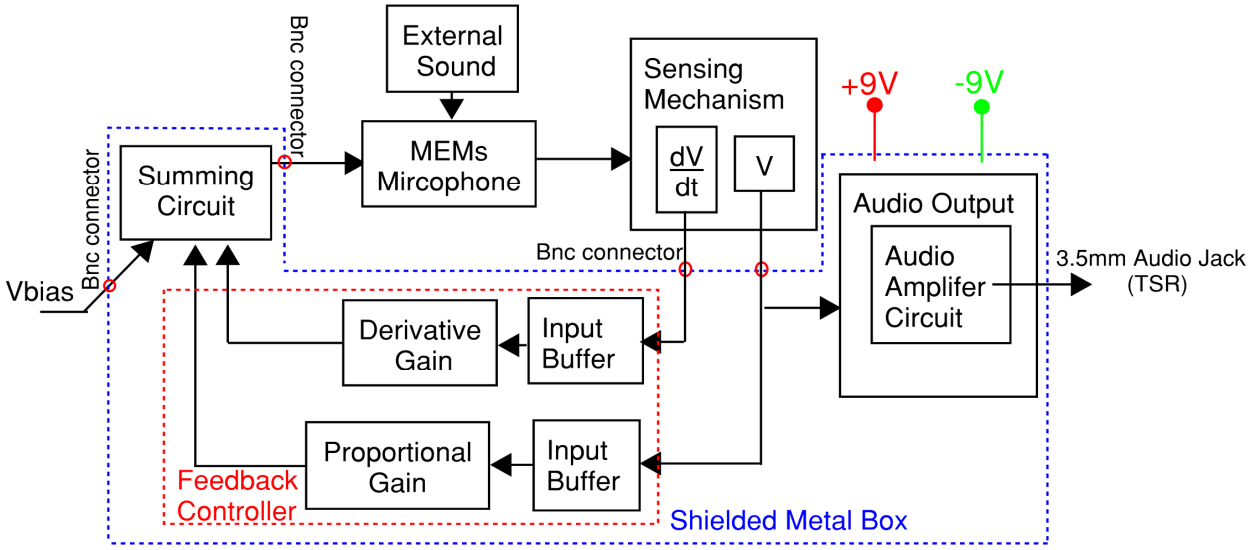

Figure 2: Overall System Block Diagram

allow the circuit to be transported easily. BNC connectors will be used to interface between the microphone's sensing mechanism and the controller. The audio output will be the standard Tip-Ring Sleeve audio jack to allow all standard headphones to be used to hear the microphone's output.

II. Analysis of problem

As mentioned in the introduction, the MEMs microphone currently has a resonant peak caused by under damping. In order to eliminate the resonance a mathematical model is needed to analyze how the microphone fundamentally operates. Equation 1 is the general differential equation associated with motion of rotation of capacitive microphones.

$$I\ddot{\theta} + c_t\dot{\theta} + k_t\theta = M + \frac{V^2}{2}\cdot\frac{\partial C}{\partial \theta} \quad (1)$$

The mass moment of inertia (I), the torsional stiffness (k_t), and the torsional dashpot constant (c_t), are constants associated with each microphone. The moment of the microphone's diaphragm, *M*, is one of the microphone's inputs. The other input of the microphone is a voltage that is converted to a moment by the properties of the microphone. Since the current sensing mechanism, the laser-vibrometer, outputs a voltage and the microphone is able to accept a voltage input, a feedback controller may be added to correct undesirable traits inherent of the microphone's small size. Although a voltage input may be applied, the voltage is squared and multiplied by the derivative of the capacitance with respect to the diaphragm's rotation. This presents two problems, how to use a squared voltage input to successfully introduce feedback and how to approximate $\frac{\partial C}{\partial \theta}$.

As described in [2], one way of handling the nonlinear voltage input is to apply a bias voltage in addition to the feedback voltage. The bias voltage sets an operating point that the microphone will rotated about. By breaking V into V_b+V_f,where V_b is the bias voltage and V_f is the feedback voltage, Equation 1 can be rewritten as:

$$I\ddot{\theta} + c_t\dot{\theta} + k_t\theta = M + \frac{{V_b}^2 + 2V_bV_f + V_f^2}{2} \cdot \frac{\partial C}{\partial \theta} \quad (2)$$

The next simplification made is to break θ into two parts, the operating point, γ_0, and rotation due to sound, δ.

$$I(\gamma_0 + \delta)'' + ct(\gamma_0 + \delta)' + kt(\gamma_0 + \delta) = M_s + \frac{{V_b}^2 + 2V_bV_f + V_f^2}{2} \cdot \frac{\partial C}{\partial \theta} \quad (3)$$

Since γ_0 does not change with time, the derivative and second derivative of γ_0 will equal 0. The remaining $k_t \cdot \gamma_0$ is equal to $\frac{{V_b}^2}{2}\frac{\partial C}{\partial \theta}$. If only small amounts of rotation around the operating point are considered, such that V_f much smaller than V_b and ${V_f}^2$ is small enough the equation becomes:

$$I\ddot{\delta} + c_t\dot{\delta} + k_t\delta = M_s + V_bV_f \cdot \frac{\partial C}{\partial \theta} \quad (4)$$

Using Equation 3 conventional linear controller design can be used. A Taylor series expansion using the first three terms is used to approximated $\frac{\partial C}{\partial \theta}$. The constants necessary for this approximation are obtained experimentally using a laser vibrometer. Assuming that $\frac{\partial C}{\partial \theta}$ is relatively constant around the operating point, it can also be considered constant in the design. Using the Taylor approximation and assuming that $\frac{\partial C}{\partial \theta}$ is relatively constant leads to the final linearized equation:

$$I\ddot{\delta} + c_t\dot{\delta} + k_t\delta = M_s + AV_bV_f \quad \text{where } A \approx \frac{\partial C}{\partial \theta} \quad (5)$$

III. Frequency Domain Analysis

In order to devise a solution that will successfully remove the resonant peak it is imperative to analyze the problem in the frequency domain. The blue line in Figure 1 shows the open loop frequency response of the MEMs microphone. The resonance which occurs at approximately 1600 Hz will cause a ringing sound at that frequency. The ideal microphone frequency response is a band pass, passing frequencies from 20 Hz to 20 kHz with a relatively constant gain. By introducing feedback the closed loop poles will be altered; if the poles are altered correctly the ideal microphone response can be obtained. The red line in Figure 3 is the bode plot of the ideal/desired closed loop frequency response.

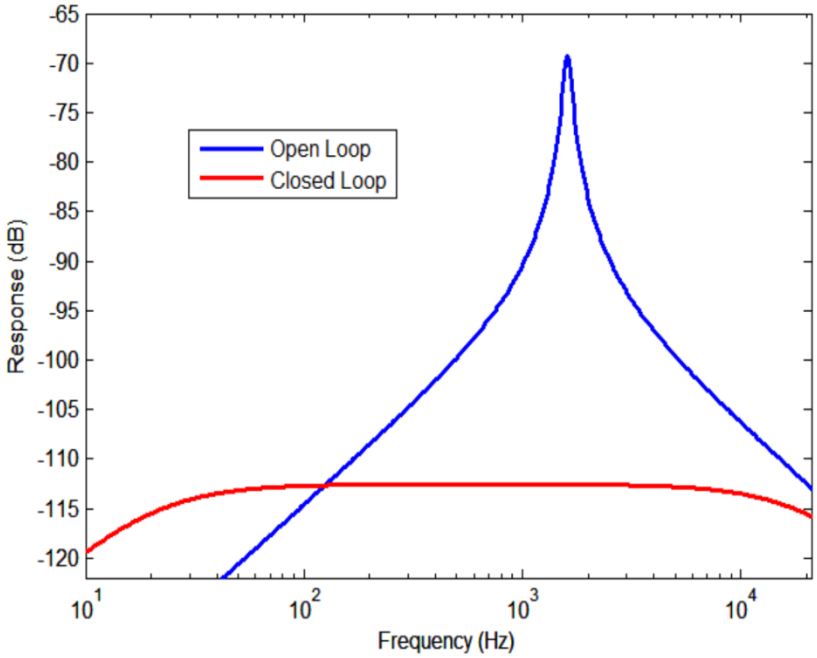

Figure 3: Frequency Response of Open Loop and Closed Loop System

IV. S Domain Controller Design

The first step in the design of a feedback controller is to derive an equation for the desired closed loop system. In this case the desired closed loop system is a band pass from 20 Hz to 20 kHz. Therefore, the system must contain a zero at 0 Hz, a pole at 20 Hz and another pole at 20 kHz. Using these guidelines the ideal/desired closed loop response is determined to be:

$$G_{desired}(s) = \frac{k \cdot s}{(s+2\pi \cdot 20) \cdot (s+2\pi \cdot 20000)} = \frac{k \cdot s}{s^2+2\pi \cdot 20020 \cdot s+4\pi^2 \cdot 400000} \quad (5)$$

Next an arbitrary controller is introduced with a 's' term and a constant term, or a PD controller. By selecting appropriate gains for the PD controller the poles can be set to the desired poles. Figure 4 shows the linear control system model of the microphone with the feedback system. Since the bias voltage and the derivative of the capacitance with respect to the rotation have both been determined to be constant in the linearized model they can simply be treated as a gain in the feedback channel. Using block diagram reduction the diagram in Figure 2 can be

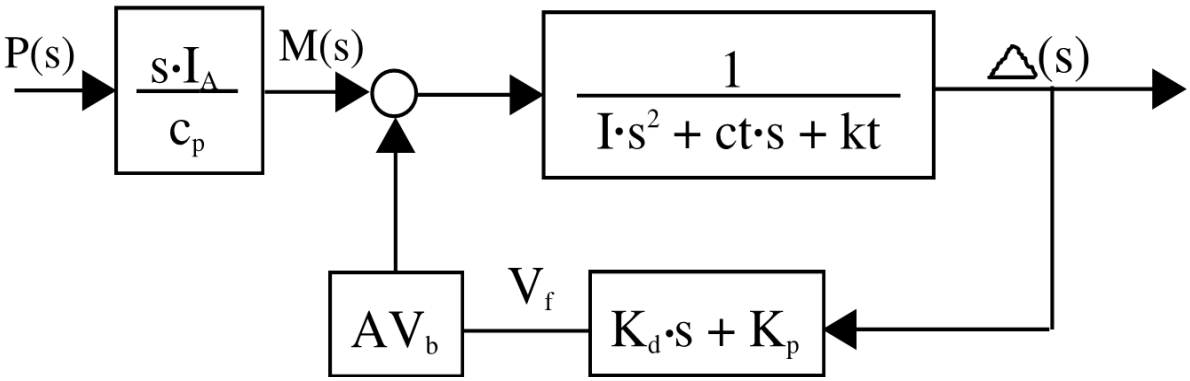

Figure 4: Linearized Control System Block Diagram

reduced to:

$$G_{cl}(s) = \frac{I_A \cdot s / c_p}{I \cdot s^2 + (ct - AV_b K_d) \cdot s + (k_t - AV_b K_p)} \quad (6)$$

Finally, to obtain the proper gains for the feedback controller (K_p and K_d), the closed loop transfer function is set equal to the desired transfer function. This yields the results:

$$K_d = \frac{c_t - I \cdot 2\pi \cdot (20020)}{AV_b} = 4.496 \quad and \quad K_p = \frac{k_t - I \cdot 4\pi^2 \cdot (400000)}{AV_b} = -3072.3 \quad (7)$$

V. Linear Simulink Model

Using the gains calculated in the previous section a Simulink model was created to simulate the frequency response of the microphone and feedback. Figure 5 is a screen capture of the linear Simulink model.

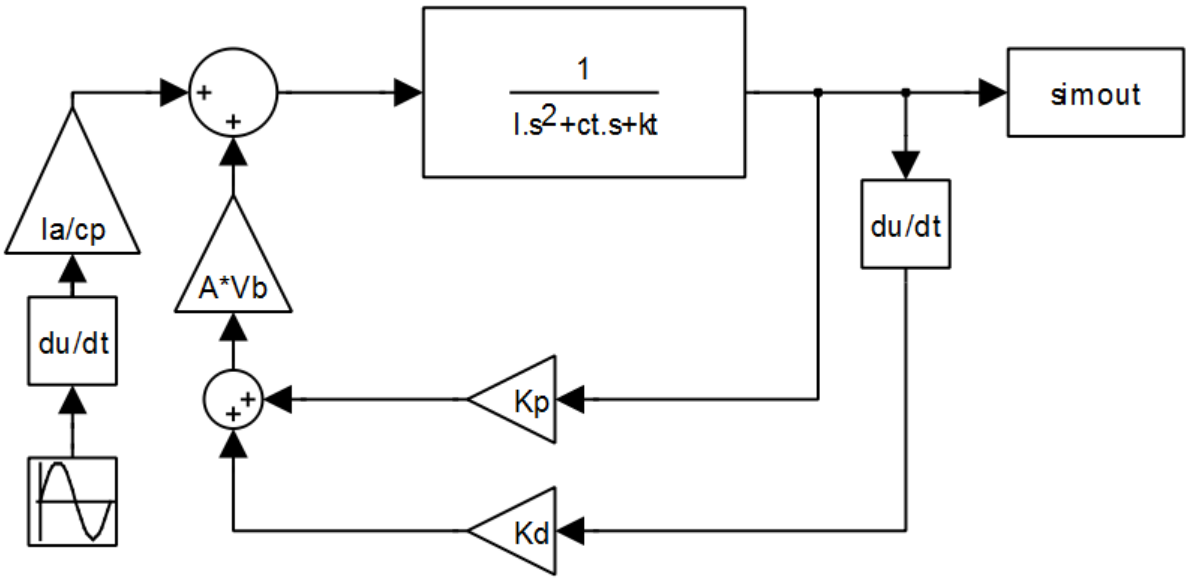

Figure 5: Linear Simulink Model

A MATLAB file sweeps the input frequency of the sine wave logarithmically from 20 Hz to 20 kHz and records the change in the steady state magnitude of the output. Figure 6 confirms that the feedback controller successfully shapes the closed loop system response to match the desired closed loop system response. This confirms that the linear design has been correct thus far. The MATLAB file used in this simulation is included in its entirety in Appendix B.

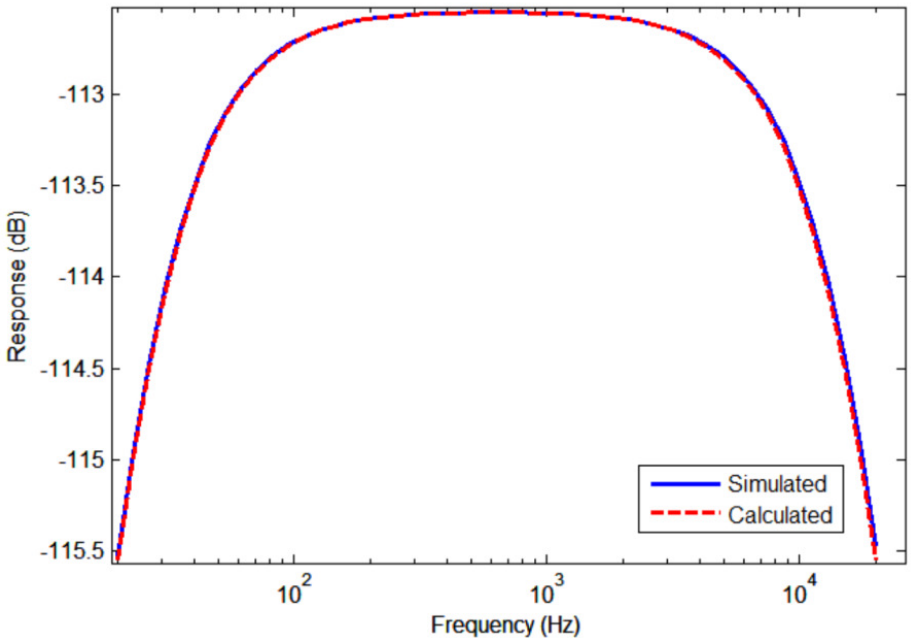

Figure 6: Simulated Closed Loop Frequency Response

VI. Parameter Variation

It is a requirement of the feedback controller to be able to be used with different variations of the MEMs microphone. As a preliminary step to meet this requirement, several theoretical calculations were performed in order to show the effects of varying parameters of the microphone. Since the controller is calculated for a specific microphone, the ideal frequency response is not expected. Although the frequency response will not be ideal, as long as the controller still successfully removes the resonance, the feedback will still greatly improve upon the open loop microphone response.

The most important parameter of the microphone is the natural frequency, $\sqrt{\frac{k_t}{I}}$. Since the natural frequency is where the resonant peak occurs, it is important to confirm that if the peak is still removed regardless of the resonance's location. To verify that the controller is capable of successfully removing the resonant peaks at several different frequencies, the variable I is varied causing the natural frequency to vary from 1100 Hz to 2200 Hz (Figure 7). The simulation code used to produce the graphs is in its entirety in Appendix C. From this simulation it can be seen that despite the change in the location of the peak, the resonance is removed.

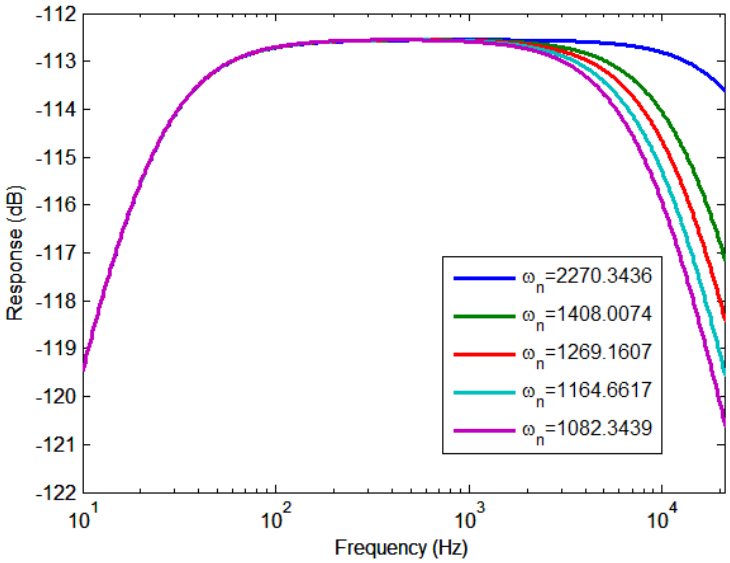

Figure 7: Closed Loop Response With Variation in I

Similarly, k_t was varied to see the effect on the closed loop system. The results corresponding to the variation of k_t are similar to the results of varying I, but the lower cutoff frequency is effected instead of the high cutoff (Figure 8).

The last parameter of the microphone that can be varied is the torsional dashpot, c_t. Since c_t does not affect where the resonance occurs it has little effect on the closed loop system, this can be easily seen in figure 9. These simulations confirm that even with significant changes in the microphone parameters the resonance peak is successfully reduced.

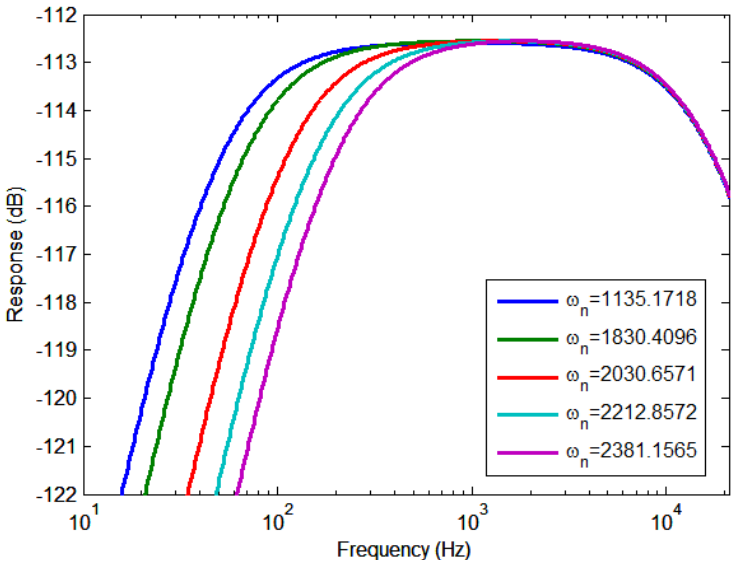

Figure 9: Closed Loop Response with Variation in k_t

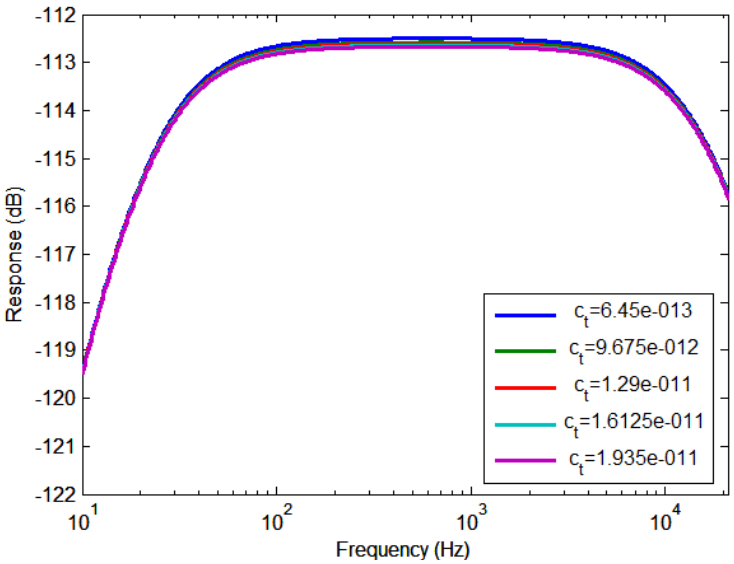

Figure 8: Closed Loop Response with Variation in c_t

VII. Noise Analysis

One of many possible applications of the MEMS microphone is that it will be used in a hearing aid. One of the most common complaints of current hearing aids is the obnoxious hissing noise that is heard in quiet conversations; therefore, one of the requirements is that the feedback controller should add no more than five decibels (5dB) of audible noise. Because of this requirement, an in-depth noise model was developed to determine how to reduce the various types of noise in the feedback controller. The analysis lead to the focus of understanding the four main kinds of noise of discrete circuit elements: flicker, shot, thermal, and burst noise.

The most commonly mentioned, and best understood, type of noise is thermal, also known as *Johnson-Nyquist*, noise. Although the average voltage across a resistor remains constant, there are variances in the voltage across a resistive circuit element, as seen in [3]. The variance of the voltage across the resistor is caused by the thermal excitation of charge carriers; the more charge carriers there are and the more exited they become, by increasing temperature, the larger the voltage variance becomes. This voltage variance, i.e., thermal noise, was analyzed by J.B. Johnson and Harry Nyquist in 1927 and can be described by $V_{therm}^{R} = \sqrt{4k_bTRW}$ where k is the Boltzmann constant, T is the temperature in Kelvin, R is resistance in ohms and W is bandwidth in Hertz. This can also be repressed as a Norton equivalent a $I_{therm}^{R} = \sqrt{\frac{4k_bTW}{R}}$. Generally, the frequency term, *W,* is not written and the thermal noise is presented in the units volts per root hertz, which is proportional to power spectral density (PSD). Because the PSD remains constant across all frequency bands, the noise is white and Gaussian who power is $P_{noise} = 4k_bTR$. The Norton and Thevenin equivalent noise circuit models are below in Figures 10 and 11, K is the Boltzmann constant.

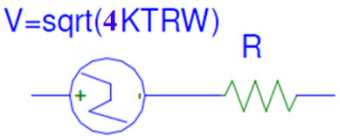

Figure 11: Thevenin Thermal Noise Model

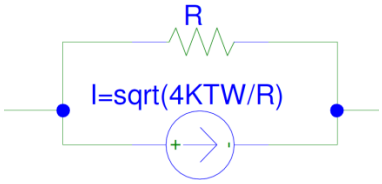

Figure 10:Norton Thermal Noise Model

At lower frequencies, usually smaller than 100 Hz, another type of noise has been observed, i.e., flickers noise. Although the source of this noise, according to [4], is not well understood, [3] disagrees and says it is related to the generation and recombination of carriers in semiconductor materials. Flicker noise is not Gaussian distributed, this can be connected to its noise power spectrum which varies as $1/f^{\alpha}$ usually where $\alpha = 1$. As seen in Figure 12, the noise spectrum of the OP470, at lower frequencies has a higher magnitude than at higher frequencies. The $1/f$ shape is indicated by the dotted line and the solid line indicates the combination of the thermal and flicker noise. Very often, flicker noise is called *pink noise* because if the power spectral density (PSD) were placed into the visual range then the noise

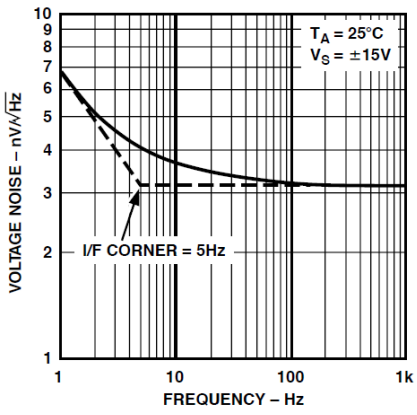

Figure 12: OP470 Flicker Noise (100Hz)

would visually be pink.

There are currently few accepted noise models for flicker noise. Looking at Figure 12, the frequency band of interest of 20 Hz to 20 kHz relative to the rest of the band, flicker noise is several orders of magnitude less than the rest of the band; however, although this is common in many operational amplifiers, it is not the case for all OpAmps.

Thermal noise generates voltage fluctuations and *shot noise* generates current fluctuations. Shot noise is present in all conducting mediums, however, it is more pronounced in semiconductor devices such as transistors and diodes as well as vacuum tubes. Elementary semiconductor theory of a PN junction, better known as a diode, states that the junction where the P and the N materials are connected there is a *depletion layer*. This layer is void of all charge carriers but still has a potential difference between the two sides of the junction.

When a voltage is applied to the ends of the PN junction, the depletion layer is made smaller and smaller increasing the number of charge carriers that *jump* from one side of the semiconductor to the other. The *average* number of charge carriers that jump is equal to the current that flows through the semiconductor device. These little jumps are, according to [3], not smooth and continuous; they are like little impulses. Shot noise is the variation in these impulses and can be calculated by $I_{sh} = \sqrt{2qI_{DC}W}$, where q is the electron charge ($1.602 * 10^{-19}\ C$), I_{DC} is the average current flowing out of the device and W is the bandwidth of interest. It should be noted that shot noise is white and Gaussian distributed.

Operational Amplifiers, along with the previously mentioned types of noise for discrete components, make of the entirety of the feedback controller. Although, fundamentally, the OpAmp consists of many subcomponents its noise model is characterized by the amplifiers input voltage noise and input current noise. This model can be seen in Figures 13 and 14, both inputs are affected by this input current (I_{n+}, I_{n-}) and voltage noise (V_{n+}, V_{n-}), keep in mind that the OpAmps in these circuits are Ideal. This model can be reduced to one voltage (V_{ni}) and current source (I_{ni}) acting on the same input, whose variance is easily found on a datasheet. These noise values follow the same flicker noise added to the white noise curve, as can be seen in Figure 12 for the OP470.

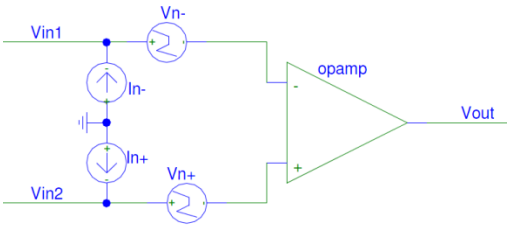

Figure 13: Amplifier Noise Model

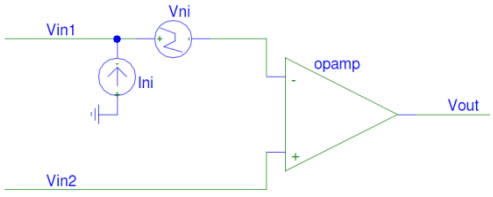

Figure 14: Reduced Noise Model

VIII. Assembling the Noise Model

Taking all of these factors into consideration, the total noise model of this system is the sum of the individual components, which are a inverting-summing amplifier and a difference amplifier models as seen in Figure 14. All terms with the subscript "*therm*" indicates its nearby resistors thermal voltage value as calculated above. The full derivation can be seen in Appendix A.

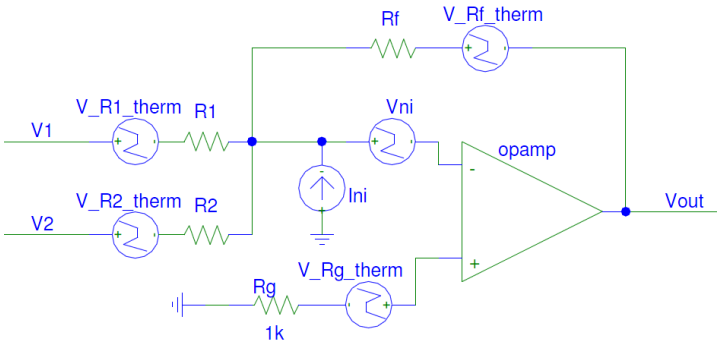

Figure 14: Summing Amplifier Noise Model

The solution for the noise voltage (that is if both V2 and V1 are zero) is:

$$V_{noise} = -\frac{R_f}{R_1}V_{therm}^{R1} - \frac{R_f}{R_2}V_{therm}^{R2} + \left(1 + \frac{R_f}{R_2} + \frac{R_f}{R_2}\right)\left(V_{ni} + V_{therm}^{Rg}\right) + V_{therm}^{R_f} + R_f I_{ni} \quad (8)$$

Be aware that this configuration can be simplified into an inverting amplifier by simply removing R_2 from the system. The result would set R_2 to infinity and eliminate all noise sources and gains related to R_2.

V_2 in this circuit is a constant bias voltage that does not require any gain, and therefore to neutralize the gain $R_2 = R_f$ and the following equation is the result:

$$V_{noise} = -\frac{R_f}{R_1}V_{therm}^{R1} - V_{therm}^{R2} + \left(2 + \frac{R_f}{R_2}\right)\left(V_{ni} + V_{therm}^{Rg}\right) + V_{therm}^{R_f} + R_f I_{ni} \quad (9)$$

Although this equation is seemingly final it is not, as these voltage values are *variances* and therefore cannot be simply summed, this will be discussed later. For now be aware that each noise source is independent from one another and therefore great care should be taken to ensure that each resistor is uniquely defined.

The second part to the MEMS microphone feedback controller is the differential amplifier, whose noise model is as seen below in Figure 15.

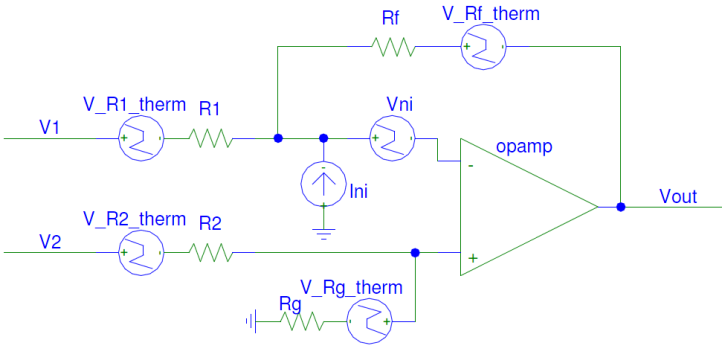

Figure 15: Difference Amplifier Noise Model

The analysis of the differential amplifier noise model yields:

$$V_{noise} = \frac{1+\frac{R_f}{R_2}}{1+\frac{R_g}{R_2}}\left(V_{therm}^{R_2}\right)\frac{R_g}{R_2} - \frac{R_g}{R_2}\left(V_{therm}^{R_1}\right) - V_{therm}^{R_f} - \left(1+\frac{R_f}{R_2}\right)V_{ni} - \frac{1+\frac{R_f}{R_2}}{1+\frac{R_g}{R_2}}\left(V_{therm}^{R_g}\right) + R_f I_{ni} \quad (10)$$

in most uses of the differential amplifier the desired equation for the system is $V_{out} = A(V_1 + V_2)$, to obtain this $R_f = R_g = R_{num}$ and $R_1 = R_2 = R_{denom}$ which yields the following:

$$V_{noise} = \frac{R_{num}}{R_{denom}}\left(V_{therm}^{R_2} - V_{therm}^{R_1}\right) - V_{therm}^{R_f} - \left(1+\frac{R_{num}}{R_{denom}}\right)V_{ni} - \left(V_{therm}^{R_g}\right) + R_{nom} I_{ni} \quad (11)$$

In order to emphasize that the noise voltage sources are independent, the appropriate label has been left on the noise voltages so that this equation does not reduce any farther. In the design for the feedback controller, this equation further reduces because $R_{num} = R_{denom}$,which results in a system gain of one and the system equation:

$$V_{noise} = \left(V_{therm}^{R_2} - V_{therm}^{R_1}\right) - V_{therm}^{R_f} - 2V_{ni} - V_{therm}^{R_g} + R_{nom} I_{ni} \quad (12)$$

and finally to relate the final equation back to the original resistor values by resetting $R_{nom} = R_f$

$$V_{noise} = \left(V_{therm}^{R_2} - V_{therm}^{R_1}\right) - V_{therm}^{R_f} - 2V_{ni} - V_{therm}^{R_g} + R_f I_{ni} \quad (13)$$

The total noise equation for the feedback controller, on page 21 Figure 23, can be calculated using equations 9 and 13. The noise through the summing and non-inverting amplifiers gets treated as if it were an input voltage source that goes into the differential amplifier. This calculation is further simplified because system gain is one and therefore the noise sources of the previous stages are unaffected. To designate the difference between all resistors, resistors with the superscript 1 correspond with the summing amplifier, those with 2 correspond to the inverting amplifier and those with 3 as their superscript correspond with the difference amplifier. The total feedback controller noise equation is as follows:

$$V_{SystemNoise} = Summing\ Amplifier - Inverting\ Amplifier + Differential\ Amplifier$$

$$V_{SystemNoise} = \left[-\frac{R_f^1}{R_1^1}V_{therm}^{R_1^1} - V_{therm}^{R_2^1} + \left(2+\frac{R_f^1}{R_1^1}\right)\left(V_{ni} + V_{therm}^{R_g^1}\right) + V_{therm}^{R_f^1} + R_f^1 I_{ni}\right] - \left[-\frac{R_f^2}{R_1^2}V_{therm}^{R_1^2} + \left(1+\frac{R_f^2}{R_1^2}\right)\left(V_{ni} + V_{therm}^{R_g^2}\right) + V_{therm}^{R_f^2} + R_f^2 I_{ni}\right] + \left[\left(V_{therm}^{R_2^3} - V_{therm}^{R_1^3}\right) - V_{therm}^{R_f^3} - 2V_{ni} - V_{therm}^{R_g^3} + R_f^3 I_{ni}\right] \quad (14)$$

Although this would seem to be the final solution, these voltage values are *uncorrelated variances,* because each noise source is independent from one another. All the noise sources are based on probability distributions, therefore cannot be summed together for a workable solution. In addition, the noise sources are Gaussian distributed values; therefore, the noise voltages can be either a positive or a negative value; this negates the importance of their sign. According to [3], the variances must be squared together to obtain the total variance of the system. Taking the

square root of the variance yields the standard deviation, which is more useful to visualize the Gaussian distribution. Therefore, this can be expressed correctly as: $V_{rms_{SystemNoise}} =$

$$\sqrt{\begin{aligned}&\left(\frac{R_f^1}{R_1^1}V_{therm}^{R_1^1}\right)^2 + \left(V_{therm}^{R_2^1}\right)^2 + \left(\left(2+\frac{R_f^1}{R_1^1}\right)V_{ni}\right)^2 + \left(\left(2+\frac{R_f^1}{R_1^1}\right)V_{therm}^{R_g^1}\right)^2 + \left(V_{therm}^{R_f^1}\right)^2 + \left(R_f^1 I_{ni}\right)^2 \\ &+ \left(\frac{R_f^2}{R_1^2}V_{therm}^{R_1^2}\right)^2 + \left(\left(1+\frac{R_f^2}{R_1^2}\right)V_{ni}\right)^2 + \left(\left(1+\frac{R_f^2}{R_1^2}\right)V_{therm}^{R_g^2}\right)^2 + \left(V_{therm}^{R_f^2}\right)^2 + \left(R_f^2 I_{ni}\right)^2 \\ &+ \left(V_{therm}^{R_2^3}\right)^2 + \left(V_{therm}^{R_1^3}\right)^2 + \left(V_{therm}^{R_f^3}\right)^2 + (2V_{ni})^2 + \left(V_{therm}^{R_g^3}\right)^2 + \left(R_f^3 I_{ni}\right)^2\end{aligned}} \quad (13)$$

A noise estimation based on modest part selection, as seen in Figure 23, yield $V_{out} = 39.3nV$ and, if the six sigma standard is used, almost all noise should fall within the range of $V_{out} = \pm 117.9nV$. To determine whether or not the system meets the customers requirement the $V_{rms_{SystemNoise}}$ must be converted Pascals and then to decibels. This conversion method is still in the process of being developed.

IX. Non-Ideal Operational Amplifier Characteristics

While researching operational amplifiers that exhibit low noise features, several points of interest were discovered that were of concern: input bias current, total harmonic distortion, gain bandwidth product and unity gain stability. Each of these could cause potential harm to the control system by obscuring the feedback signals.

Although theoretical operational amplifiers have no current flowing into the inverting and non-inverting terminals, in reality there is a small current flowing into the amplifier. This current flow is not a noise with variance, but rather this input bias current, as it is called, is a steady flow regardless of the gain of the system. Looking at the circuit diagram in Figure 16, the bias current is modeled by flowing into both terminals.

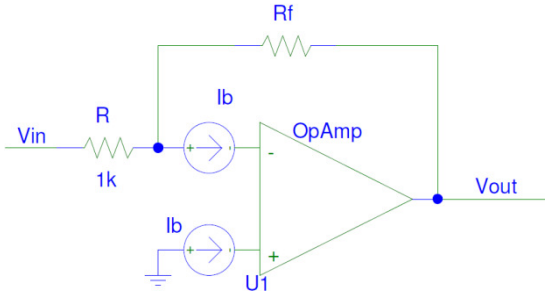

Figure 16: Inverting Amplifier with Input Bias Current

If the input is grounded, the input bias current will generate a constant output voltage $V_{out} = R_f I_b$. If both R_f and I_b are considerable values and the input signal is small it will be buried by this "voltage floor." Fortunately, this issue can be easily taken care of by inserting a balancing resistor at the non-inverting terminal, as shown below in Figure 17.

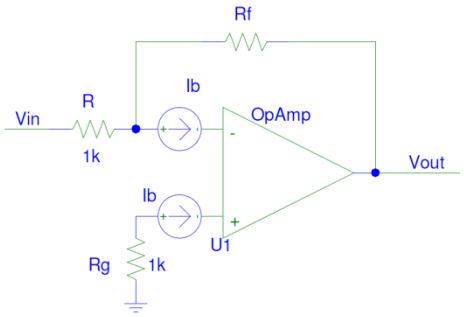

Figure 17: Inverting Amplifier with Balancing Resistor

The solution to this system is: $V_{out} = -\left(1 + \frac{R_f}{R}\right) I_b R_g + R_f I_b$ if solved for R_g when $V_{out} = 0$, then $R_g = \frac{R_f R}{R_f + R}$. In other words, if R_g is the parallel combination of R and R_f, then the voltage generated by the input bias current is eliminated.

The secondary issue of operational amplifiers is the *Total Harmonic Distortion* (THD). THD is defined as the ratio of the sum of the power of all harmonics above the fundamental frequency divided by the power of the fundamental frequency, or simply:

$$THD = \frac{\sum Harmonic\ Powers}{Fundamental\ Frequency\ Power} * 100 = 20 \log\left(\frac{\sqrt{V_2^2 + V_3^2 + \cdots + V_n^2}}{V_1}\right)$$

This is expressed as a percentage and often is described in terms of decibels. What can potentially make THD devastating to the system is that it can distort a signal from one shape to another. For example, if enough harmonics are added to a sine wave, then its shape will change into a square wave. More importantly, it can misshape the desired control effort applied by the MEMS microphone controller.

Generally, THD characteristics of most amplifiers start at as small as -40 dB and can go as low as -120 dB, or in other words, 0.01% or as low as $10^{-6}\%$ distorition. If the distortion of the control signal is disregarded and if the output is thought of as an audio signal, according to [5], human cannot discernibly hear distortion less than or equal to 1%. Therefore, THD was determined not to be a source of concern after looking at typical operational amplifier data sheets.

During the early stages of prototyping the feedback controller, it was discovered that the bandwidth was not sufficient at the required gain. The culprit to this issue is the Gain Bandwidth Product of the operational amplifiers used in prototyping. The general transfer function of an operational amplifier is a first, sometimes second, order low pass filter. The Gain Bandwidth Product (GBP) is a constant such that $GBP = Gain * Bandwidth$; therefore, as the gain of the system increases the bandwidth decreases and vice versa. The GBP is defined as the frequency for which the output for the open loop gain is 0 dB. This problem can be easily overcome by correctly choosing an operational amplifier that has a larger GBP.

Well informed with the previous information, the AD797 was chosen. The AD797 has less than $1nV/\sqrt{Hz}$ voltage input noise, gain bandwidth product of 8 MHz, and harmonic distortion of $-120dB$. However, as perfect as this chip could be it had one fatal flaw, the AD797 is not unity gain stable on breadboards. Unity gain stability means that the amplifier can operate at a gain of one and not have any discernable issues with the output. When a sinusoid is inputted into the AD797 at unity gain, the output was distorted by a constantly fluctuating square wave-like shape. It was an inaccurate representation of the input signal. Unity gain stability extends farther, even gains of less than ten, the input signal is distorted by the amplifier. Some amplifiers are explicitly marked as stable at gains above some value to ensure the user is aware of the capabilities of the amplifier.

X. Part Selection

Armed with the arsenal of information about the undesirable characteristics of operational amplifiers, a decision matrix was used to select the optimal amplifier. The following criteria were used in the selection process: Does the chip come in both DIP and SOIC format, so that breadboard prototyping may be done as well as a final PCB design? Is it single package or quad package? Is the chip Unity Gain Stable? How large is the Gain Bandwidth Product, input voltage noise, input current noise and total harmonic distortion?

Charts A and B in Appendix A, Chart A lists all the critical elements of the operational amplifiers and how much weight they are worth in the overall selection. Chart B shows the number of percentage points that each term receives. Overall the winner was the OP470, but because of how close the OP470 is to the AD743 samples of both were requested from the manufacturer; unfortunately, the AD743 has been marked obsolete and samples were not available.

XI. Audio Output Design

A requirement of the system is to include an audio circuit to allow the microphone output to be heard using standard headphones. This audio output must be designed with a control knob that allows for adjustable volume with a gain that can reach zero. The input to the audio output circuit will be the proportional output of the sensing mechanism connected to the microphone. The output of the audio circuit will use the standard Tip-Ring Sleeve socket.

The audio output circuit was initially designed around the LM386 Low Voltage Audio Amplifier IC which would be powered by the 9V battery. It contains an internal gain that is set to 20. This would avoid multiple external parts and allow the design to be compact.

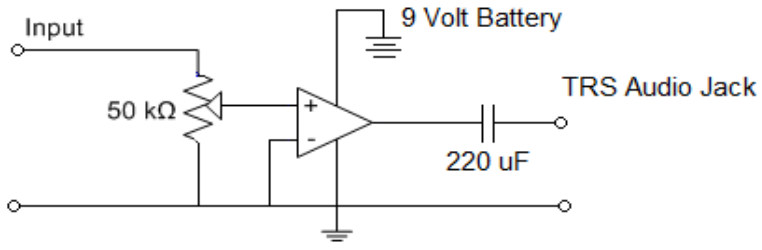

Figure 18: Audio Design With LM386

The input to the circuit is the proportional output from the laser-vibrometer. It is passed through a 50 kΩ potentiometer which controls the input signal level and creates the adjustable volume control knob. Figure 19 shows the circuit configuration.

During the development of the controller, it was realized that not all of the OpAmps in the quad-package OP470 were used. The audio output was redesigned to utilize an unused OpAmp on the quad package. This would allow for a more compact design by not needing the extra 8-pin package of the LM386. The high performance of the OP470 is also ideal for being an audio amplification OpAmp.

The revised circuit uses a non-inverting OpAmp configuration with a potentiometer in the feedback as seen in Figure 20.

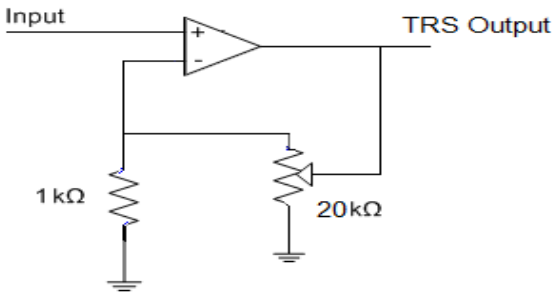

Figure 19: First Revision of Audio Design

The 20 kΩ potentiometer allows for a maximum gain of 21 and for control of the voltage level and is therefore used for a volume control knob. Two problems were discovered in this design. First, the minimum gain is one which means the sound cannot be turned off completely. Second, placing a potentiometer in the feedback of an OpAmp produces more noise.

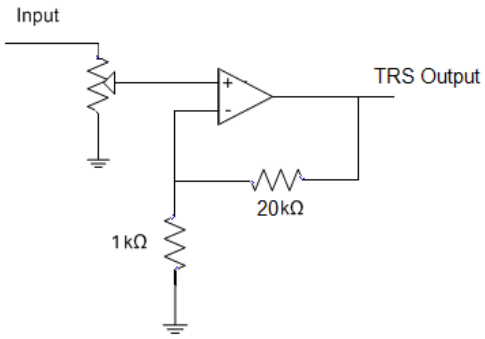

Figure 20: Final Design of Audio Output

The final revision of the audio output circuit also uses the non-inverting OpAmp configuration seen in Figure 21. The feedback potentiometer is replaced with a 20 kΩ resistor to

create a maximum gain of 21 and the potentiometer is placed at the input of the circuit to control the input voltage level and is used as the volume control.

The output of the circuit is connected to a TRS 3.5mm 1/8 inch socket which has two channels. Although the microphone output is single channel, the decision to use two channels was made to allow a wide variety of headphones and speakers to be used with the audio output circuit. Both channels of the TRS jack will output the signal of the audio output circuit.

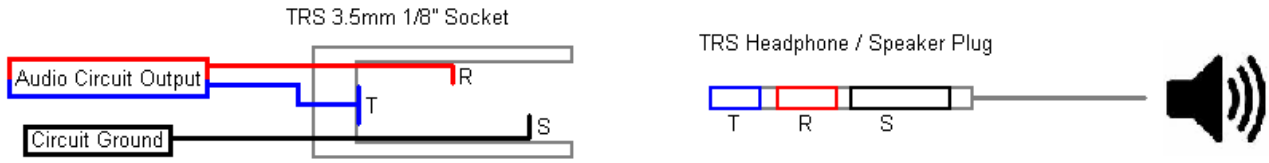

Figure 21: Tip-Ring Sleeve Connections

XII. Chassis

Another concern of this project is the effects of outside signals such as electromagnetic interference. Since the voltage signal levels within the feedback controller must have low noise, it is necessary to eliminate outside interference. Although most common EMI transmission occurs at frequencies from 50 MHz to 500 MHz, the feedback controller is mainly concerned with EMI transmissions with frequencies within the audible range, such as 60 Hz EMI from power lines.

An initial solution to the problem was to introduce an Anti-hum filter, a notch filter that does not pass frequencies from 59-61 Hz. However, this may still allow higher harmonics of the 60Hz to be present.

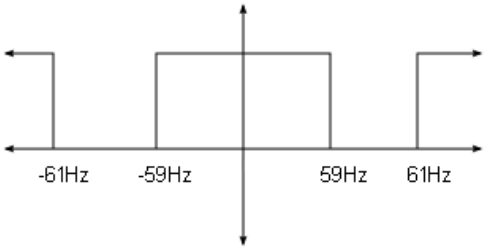

Figure 22: Ideal Anti-Hum Filter

A simpler and more effective solution is to surround the circuit in a metallic case which would eliminate all forms of outside electromagnetic interference without adding more circuit components. The prototype circuit on the breadboard is surrounded by a premade metal chassis that fits the dimensions of the requirements. Designing a custom chassis for the prototype would be a drain on the project budget and is not necessary for the prototype. It is fitted with BNC connectors to connect to the testing equipment used by Professor Miles. After the final build of the circuit is completed on a PCB, a custom metal chassis will be designed and fabricated for the device.

XIII. Implementation

The prototype of the feedback controller and audio circuit was built on a breadboard and uses the OP470 OpAmp. The final prototype design schematic is shown in Figure 24.

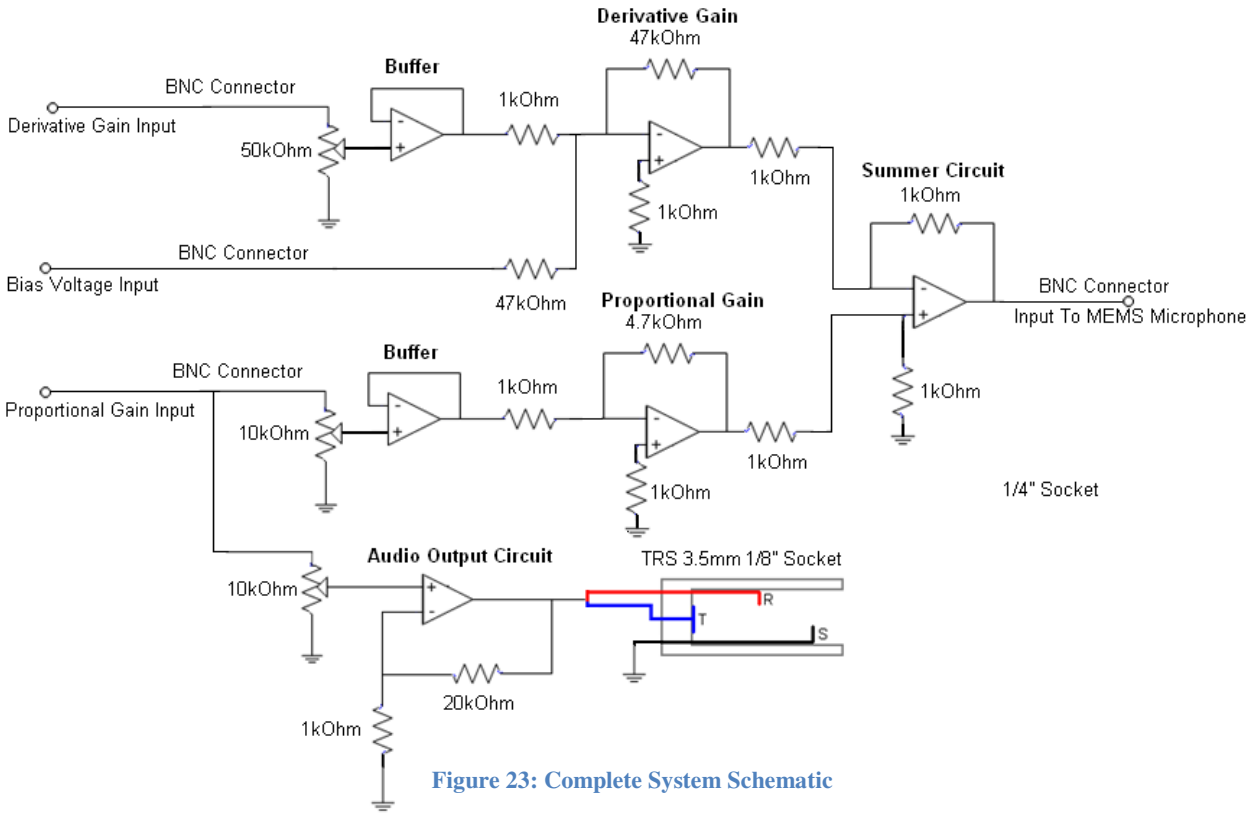

Figure 23: Complete System Schematic

After taking into consideration the sensor gains, the gains for the derivative input and proportional input were calculated to be approximately 45 and -3.1 respectively. Therefore, using standard resistor values, a maximum gain of 47 was chosen for the derivative input and a gain of 4.7 was chosen for the proportional input. The proportional gain is made negative by being subtracted in the summer circuit. It was deliberately chosen to be larger than the calculated gains to allow for variations of the microphones made during fabrication. The three inputs to the control system and the output are all connected via BNC connectors as stated in the requirements since Professor Miles's test equipment uses BNC connectors. Testing of the system will begin early next year.

XIV. Conclusion

The feedback controller was designed to eliminate the resonant peak in the frequency response of the MEMS microphone. The feedback circuit was designed as a Proportional-Derivative controller and was created with adjustable parameters to allow for compatibility with variations in the microphones that occur during manufacturing. Simulink models of the microphone and feedback controller have shown that the PD controller is capable of reducing the

resonant peak of the MEMS microphone. As a bridge step to the PD controller, a summer circuit was prototyped on a breadboard. The summer circuit has three inputs, a proportional input and a derivative input from the laser vibometer, and an input bias. The output of controller feeds back into the MEMS microphone to correct the resonant peak. The controller also contains an audio output circuit which allows for standard 3.5 mm 1/8 inch TRS headphones or speakers to output sound from the microphone. Extensive noise research was done to ensure that the design of the controller would not generate a substantial amount of noise that would interfere with its operation. Testing of the prototype will begin early next semester. It is also expected that an optical sensing mechanism will be introduced to replace the laser-vibrometer. The PD controller parameters will need to be adjusted to be compatible with the new sensing mechanism. The final design is planned to be placed on a PCB and enclosed by a fabricated metal chassis.

APPENDIX A: Noise Derivations

Summing Amplifier:

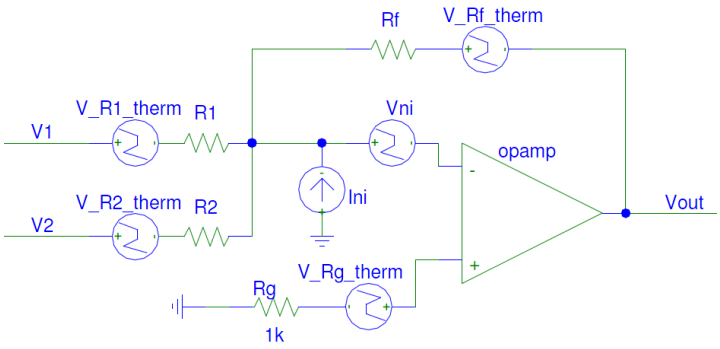

Figure 24: Summing Amplifier Noise Model

$$V_{node} = V_{NI} + V_{therm}^{Rg}$$
(1)

$$0 = \frac{V_1 + V_{therm}^{R1} - V_{node}}{R_1} + \frac{V_2 + V_{therm}^{R2} - V_{node}}{R_1} + \frac{V_{out} + V_{therm}^{Rf} - V_{node}}{R_f} + I_{NI}$$
(2)

$$0 = \frac{R_f}{R_1}(V_1 + V_{therm}^{R1} - V_{node}) + \frac{R_f}{R_2}(V_2 + V_{therm}^{R2} - V_{node}) + V_{out} + V_{therm}^{Rf} - V_{node} + R_f I_{NI}$$
(3)

$$V_{out} = \frac{R_f}{R_1}(V_1 + V_{therm}^{R1} - V_{node}) + \frac{R_f}{R_2}(V_2 + V_{therm}^{R2} - V_{node}) + V_{out} + V_{therm}^{Rf} - V_{node} + R_f I_{NI}$$
(4)

$$V_{out} = -\frac{R_f}{R_1}(V_1 + V_2) - \frac{R_f}{R_1}V_{therm}^{R1} - \frac{R_f}{R_2}V_{therm}^{R2} + \left(1 + \frac{R_f}{R_1} + \frac{R_f}{R_2}\right)V_{node} - V_{therm}^{Rf} - R_f I_{NI}$$
(5)

Substituting Equation 1 into Equation 5

$$V_{out} = -\frac{R_f}{R_1}(V_1 + V_2) - \frac{R_f}{R_1}V_{therm}^{R1} - \frac{R_f}{R_2}V_{therm}^{R2} + \left(1 + \frac{R_f}{R_1} + \frac{R_f}{R_2}\right)(V_{NI} + V_{therm}^{Rg}) - V_{therm}^{Rf} - R_f I_{NI}$$ (6)

Eliminate all terms that do not effect noise.

$$V_{noise} = -\frac{R_f}{R_1}V_{therm}^{R1} - \frac{R_f}{R_2}V_{therm}^{R2} + \left(1 + \frac{R_f}{R_1} + \frac{R_f}{R_2}\right)(V_{NI} + V_{therm}^{Rg}) - V_{therm}^{Rf} - R_f I_{NI}$$
(7)

Difference Amplifier:

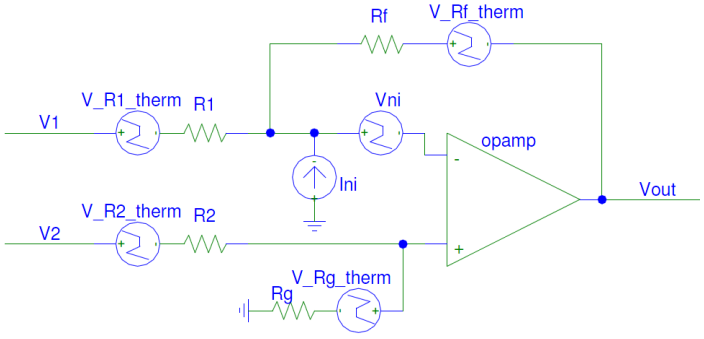

Figure 25: Difference Amplifier Noise Model

For the V^+ terminal:

$$0 = \frac{V_2 + V_{therm}^{R2} - V^+}{R_2} + \frac{V^+ - V_{therm}^{Rg}}{R_g} \quad (1)$$

$$0 = \frac{R_g(V_2 + V_{therm}^{R2} - V^+)}{R_2} + V^+ - V_{therm}^{Rg} \quad (2)$$

$$\frac{R_g(V_2 + V_{therm}^{R2})}{R_2} - V_{therm}^{Rg} = \left(1 + \frac{R_g}{R_2}\right) V^+ \quad (3)$$

$$V^+ = \frac{\frac{R_g}{R_2}(V_2 + V_{therm}^{R2}) - V_{therm}^{Rg}}{\left(1 + \frac{R_g}{R_2}\right)} \quad (4)$$

Solving for V_{out}

$$V_{node} = V^+ + V_{NI} \quad (5)$$

$$0 = \frac{V_1 + V_{therm}^{R1} - V_{node}}{R_1} + \frac{V_{out} + V_{therm}^{Rf} - V_{node}}{R_f} + I_{NI} \quad (6)$$

$$0 = \frac{R_f}{R_1}(V_1 + V_{therm}^{R1}) - \frac{R_f}{R_1} V_{node} + V_{out} + V_{therm}^{Rf} - V_{node} + R_f I_{NI} \quad (7)$$

$$0 = \frac{R_f}{R_1}(V_1 + V_{therm}^{R1}) - \left(1 + \frac{R_f}{R_1}\right) V_{node} + V_{out} + V_{therm}^{Rf} + R_f I_{NI} \quad (8)$$

$$V_{out} = \frac{R_f}{R_1}(V_1 + V_{therm}^{R1}) - \left(1 + \frac{R_f}{R_1}\right) V_{node} + V_{therm}^{Rf} + R_f I_{NI} \quad (9)$$

$$V_{out} = \frac{R_f}{R_1}(V_1 + V_{therm}^{R1}) - \left(1 + \frac{R_f}{R_1}\right) V_{node} + V_{therm}^{Rf} + R_f I_{NI} \quad (10)$$

combining Equations 4, 5 and 10 and simplifying

$$V_{out} = \frac{R_g}{R_2}\left(\frac{1 + \frac{R_f}{R_1}}{1 + \frac{R_g}{R_2}}\right) V_2 - \frac{R_f}{R_1} V_1 + \frac{R_g}{R_2}\left(\frac{1 + \frac{R_f}{R_1}}{1 + \frac{R_g}{R_2}}\right) V_{therm}^{R2} - \frac{R_f}{R_1} V_{therm}^{R2} + \left(\frac{1 + \frac{R_f}{R_1}}{1 + \frac{R_g}{R_2}}\right) V_{therm}^{Rg} + \left(1 + \frac{R_f}{R_1}\right) V_{NI} - V_{therm}^{Rf} - R_f I_{NI} \quad (11)$$

Eliminate all voltages that are not noise

$$V_{out} = \frac{R_g}{R_2}\left(\frac{1 + \frac{R_f}{R_1}}{1 + \frac{R_g}{R_2}}\right) V_{therm}^{R2} - \frac{R_f}{R_1} V_{therm}^{R2} + \left(\frac{1 + \frac{R_f}{R_1}}{1 + \frac{R_g}{R_2}}\right) V_{therm}^{Rg} + \left(1 + \frac{R_f}{R_1}\right) V_{NI} - V_{therm}^{Rf} + R_f I_{NI} \quad (12)$$

APPENDIX B: Decision Matrices

Chart A

Chip	Weight	AD797	AD743	OP470	TL0748CN	AD548	Units
Input Noise	0.10	1.0	2.9	3.2	15	30	nV/√Hz
Input Noise	0.20	2000	6.9	1700	10	1.8	fA/√Hz
THD	0.05	-120 0.0001	-100 0.0003	-80 0.001	-100 0.0003	-73 0.003	dB %
Gain BW Product	0.20	8	4.5	6	3	1	MHz
Unity Gain Stable	0.30	0.25	1	1	1	1	Yes = 1 No = 0
Packaging	0.15	1	1	4	4	1	Amps/Pack

Chart B

Chip	Weight	AD797	AD743	OP470	TL0748CN	AD548
Input Noise	10%	10	9	8	5	3
Input Noise	20%	10	16	10	14	18
THD	5%	5	4.75	4	4.75	3.5
Gain BW Product	20%	20	16	18	8	2
Unity Gain Stable	30%	7.5	30	30	30	30
Packaging	15%	7.5	7.5	15	15	7.5
Total	**100%**	**60**	**83.25**	**85**	**76.75**	**64**

APPENDIX C: Matlab Gain Calculations and Parameter Calculation

```
%gain calculations and parmeter variation
%Kp=-4733;
%Kd=4.465;
clear
kt=7.58e-7;%N*m/rad
a=-9.7549e-11; b=-5.9191e-8; c=2.1503e-5; %dC/dTe approximation
Vb=3; %Volts
I=7.45e-15; %kg m^2
ct=6.45e-12; %N*m*s/rad
Ia=7.65e-13; %m^4
beta=20000*(2*pi); %Hz
alpha=20*(2*pi); %Hz
cp=344; %m/s
syms g0;%solve for gamma0
x=Vb^2/2;
k=sym2poly(solve(x*c*(g0^2)+((x*b-kt)*g0)+x*a,g0));
%check if Vb=0 will give open loop response
A=a+b*k(1)+c*k(1)^2;
syms s;
Kd=(ct-(I*(alpha+beta))/(A*Vb));
Kp=(kt-I*alpha*beta)/(A*Vb);
Vb=3;
Gdesired_den=sym2poly(s^2+s*(alpha+beta)+alpha*beta);
Gcalc_den=sym2poly((I*s^2+((ct)-A*Vb*Kd)*s+(kt)-A*Vb*Kp));
Gcalc=tf([Ia/(cp) 0],Gcalc_den);
Gdesired=tf([beta 0],Gdesired_den);
%bode(Gcalc);
%%examine the parameter changes
freqmin=.1*2*pi;
freqmax=2*pi*25000;
numfreq=1000;
freq=logspace(log10(freqmin),log10(freqmax),numfreq);
omega=2*pi*freq;
s=j*omega;
Gol=Ia*s/cp./(s.^2*I+kt+s*ct);
Gcl=(Ia*s/cp)./(I*s.^2+((ct)-A*Vb*Kd)*s+(kt)-A*Vb*Kp);
Kp_cur=Kp;
for i=1:5;
    G(:,i)=20*log10(abs((Ia/cp)*s./(I*s.^2+((ct)-A*Vb*Kd)*s+(kt)-
A*Vb*Kp_cur)));
    Kp_dat(i,:)=sprintf('Kp=%i',Kp_cur);
    Kp_cur=Kp+Kp*.2*i;
end
figure(1);
semilogx(freq,G(:,1),freq,G(:,2),freq,G(:,3),freq,G(:,4),freq,G(:,5),freq,20*
log10(abs(Gol)),'linewidth',2);
title 'Kp effect on closed loop response';
xlabel 'Frequency (Hz)'; ylabel 'Response (dB)';
legend(Kp_dat);
axis([.1 21000 -122 -65]);
Kp=(kt-I*alpha*beta)/(A*Vb);
Kd_cur=Kd;
for i=1:5;
    G(:,i)=20*log10(abs((Ia/cp)*s./(I*s.^2+((ct)-A*Vb*Kd_cur)*s+(kt)-
A*Vb*Kp)));
```

```
    Kd_dat(i,:)=sprintf('Kd=%f',Kd_cur);
    Kd_cur=Kd-Kd*(.10*i);
    end
figure(2);
semilogx(freq,G(:,1),freq,G(:,2),freq,G(:,3),freq,G(:,4),freq,G(:,5),freq,20*
log10(abs(Gol)),'linewidth',2);
legend(Kd_dat);
title 'Kd effect on closed loop response';
xlabel 'Frequency (Hz)'; ylabel 'Response (dB)';
axis([10 21000 -122 -65]);
kt_cur=.5*kt;
for i=1:5
    G(:,i)=20*log10(abs((Ia/cp)*s./(I*s.^2+((ct)-A*Vb*Kd)*s+(kt_cur)-
A*Vb*Kp)));
    wo=sqrt(kt_cur/I)/(2*pi);
    wo_dat(i,:)=wo;
    kt_d(i,:)=kt_cur;
    kt_cur=kt_cur+.25*kt*i;
end;
figure(3);
semilogx(freq,G(:,1),freq,G(:,2),freq,G(:,3),freq,G(:,4),freq,G(:,5),'linewid
th',2);
xlabel 'Frequency (Hz)'; ylabel 'Response (dB)';
axis([10 25000 -122 -112]);
legend(num2str(kt_d));

ct_cur=.5*ct;
for i=1:5
    G(:,i)=20*log10(abs((Ia/cp)*s./(I*s.^2+((ct_cur)-A*Vb*Kd)*s+(kt)-
A*Vb*Kp)));
    ct_s(i,:)=ct_cur;
    ct_cur=ct_cur+.25*ct*i;
end;
figure(4);
semilogx(freq,G(:,1),freq,G(:,2),freq,G(:,3),freq,G(:,4),freq,G(:,5),'linewid
th',2);
xlabel 'Frequency (Hz)'; ylabel 'Response (dB)';
legend(num2str(ct_s));
axis([10 25000 -122 -112]);

I_cur=.5*I;
for i=1:5
    G(:,i)=20*log10(abs((Ia/cp)*s./(I_cur*s.^2+((ct)-A*Vb*Kd)*s+(kt)-
A*Vb*Kp)));
    wo=sqrt(kt/I_cur)/(2*pi);
    wo_dat(i,:)=wo;
    I_d(i,:)=I_cur;
    I_cur=I_cur+.25*I*i;
end;
figure(5);
semilogx(freq,G(:,1),freq,G(:,2),freq,G(:,3),freq,G(:,4),freq,G(:,5),'linewid
th',2);
xlabel 'Frequency (Hz)'; ylabel 'Response (dB)';
axis([10 25000 -122 -112]); legend(num2str(I_d));
```

APPENDIX D: Simulink Linear Model

```
%Simulink Linear Model
%define Constants
clear;
kt=7.58e-7;%N*m/rad
a=-9.7549e-11; b=-5.9191e-8; c=2.1503e-5; %dC/dTe approximation
Vb=3; %Volts
I=7.45e-15; %kg m^2
ct=6.45e-12; %N*m*s/rad
Ia=7.65e-13; %m^4
beta=20000*(2*pi); %Hz
alpha=20*(2*pi); %Hz
cp=344; %m/s
syms g0;
F=logspace(log10(20),log10(20000),50);
jw=2*pi*F*i;
%solve for gamma0
x=Vb^2/2;
k=sym2poly(solve(x*c*(g0^2)+((x*b-kt)*g0)+x*a,g0));
A=a+b*k(1)+c*k(1)^2;
g0=k(1);
syms s;
Kd=(ct-(I*(alpha+beta))/(A*Vb));
Kp=(kt-I*alpha*beta)/(A*Vb);
load_system('mic_with_feedback');
amp=1;
k=1;
for i=1:length(F)
    Tsim=floor(900*I/ct)/5; %Tset=4/(2*(ct/I))<<Tsim
    Fs=20000*40;
    ts=1/Fs;
    f=F(i);
    sim('mic_with_feedback');
    H(i)=((max(simout(.7*length(simout):length(simout)))-
(min(simout(.7*length(simout):length(simout)))))/2)/amp;
end
semilogx(F,20*log10(abs(H)),F,20*log10(abs((Ia/cp)*(jw)./(I*jw.^2+jw*(ct-
A*Vb*Kd)+(kt-A*Vb*Kp)))),'r--','linewidth',2);
xlabel 'Frequency (Hz)', ylabel 'Response (dB)';
```

APPENDIX E: Schedule

Task Name	Responsible Party		Week of: 31-Aug	6-Sep	13-Sep	20-Sep	27-Sep	4-Oct	11-Oct	18-Oct	25-Oct	1-Nov	8-Nov	15-Nov	22-Nov	29-Nov	6-Dec
Differential Equation Analysis	Andrew Steinmann	Exp			15%	55%	85%	100%									
		Act			20	50	75	90	100								
Circuit Design (PD)	Andrew Steinmann	Exp			10%	20%	30%	40%	50%	65%	80%	95%	100%				
		Act			10	25	35	45	55	65	80	95	100				
Simulink Modeling	Andrew Steinmann	Exp								25%	50%	75%	100%				
		Act								20	50	80	100				
Matlab Parameter Analysis	Andrew Steinmann	Exp									20%	40%	60%	80%	100%		
		Act									20	40	60	80	100		
MEMS microphone research	Wesley Chiu	Exp		30%	60%	100%											
		Act		30	60	100											
Prototyping Summer Circuit	Wesley Chiu	Exp						10%	20%	40%	60%	80%	100%				
		Act						10	25	35	60	80	95				
Pspice Model of controller	Wesley Chiu	Exp								10%	30%	50%	70%	90%	100%		
		Act								5	30	50	70	90	100		
Audio Output Design	Wesley Chiu	Exp					15%	35%	45%	65%	75%	90%	100%				
		Act					10	30	45	55	80	90	100				
Chasis Design	Wesley Chiu	Exp										30%	50%	75%	100%		
		Act										30	50	65	75		

Op Amp Research and Selection	Adam Hess	Exp		25%	40%	50%	75%	85%	100%	100%	100%	
		Act		25	40	50	75	90	90	90	100	
Noise Performance Analysis	Adam Hess	Exp		10%	20%	30%	40%	50%	65%	80%	95%	100%
		Act		10	25	35	45	55	65	80	95	100
Circuit design	Adam Hess	Exp	10%	20%	30%	40%	50%	65%	80%	95%	100%	
		Act	10	25	35	45	55	65	80	95	100	
Pspice Model	Adam Hess	Exp				20%	35%	40%	50%	60%	75%	100%
		Act				35	35	35	50	80	80	100
Implementing & Testing	Andrew Steinmann, Wesley Chiu, Adam Hess	Exp						10%	25%	45%	65%	85%	100%
		Act						10	35	45	80	80	80

APPENDIX F: Budget

Costs of Labor:

	Name	Task Name (must line up with your schedule)		Estimated Hours
1		Op Amp Research		25
2		Noise Performance Analysis		35
3		Circuit design		15
4		Pspice Model		5
5		Implementing & Testing (Circuits)		20
			Total Hours	100
	Adam Hess		Total Labor Cost	$10,000.00
1		Prototyping Summer Circuit		20
2		Pspice Model of controller		30
3		Implementing & Testing (Circuits)		20
4		Chasis Design		15
5		MEMS microphone research		15
6		Audio Output Design		20
			Total Hours	120
	Wesley Chiu		Total Labor Cost	$12,000.00
1		Differential Equation Analysis		10
2		Circuit Design (PD)		20
3		Simulink Modeling		25
4		Implementing & Testing (Circuits)		20
5		Matlab Parameter Analysis		15
			Total Hours	90
	Andrew Steinmann		Total Labor Cost	$9,000.00
			Total Project Labor Costs	**$31,000.00**

Actual Cost of Parts:

Item #	Item Name	P/N (if applicable)	Cost / unit	Qanity	Total Cost
1	9v battery		$3.00	2	$6.00
2	AD797 (Free Samples)		$8.76	15	$0.00
3	Resistors (330 pcs)		$8.00	1	$8.00
4	Capacitors		$0.50	5	$2.50
5	TL084 Op Amp	296-1784-5-ND	$0.88	5	$4.40
6	Oscilloscope (Owned by school)				$0.00
7	Power Supply (Owned by school)				$0.00
8	Function generator (Owned by school)				$0.00
9	Matlab (School License)				$0.00
10	Audio Jack 3.5mm 1/8"		$3.00	1	$3.00
				Total	**$23.90**

Commercial Cost of Parts:

Item #	Item Name	P/N (if applicable)	Cost / unit	Quantity	Total Cost
1					$0.00
2	9v battery		$3.00	2	$6.00
3	AD797		$8.76	15	$131.40
4	Resistors (330 pcs)		$8.00	1	$8.00
5	Capacitors		$0.50	5	$2.50
6	TL084 Op Amp	296-1784-5-ND	$0.88	5	$4.40
7	Oscillascope (Owned by school)				$0.00
8	Power Supply (Owned by school)			1	$0.00
9	Function generator (Owned by school)				$0.00
10	Audio Jack 3.5mm 1/8"		$3.00	1	$3.00
			Total Materials		**$155.30**

Total Project Costs (fall)	$31,155.30

References:

[1] R. N. Miles et al, "A low-noise differential microphone inspired by the ears of the parasitoid fly Ormia ochracea", ME Dept. Binghamton University, January 2009
[2] R. N. Miles and Q. T. Su, "Differential MEMS Microphone with Active Q-Control", ME Dept. Binghamton University, October 2009
[3] C.D. Mochenbacher, *Low-Noise Electonic System Design*, New York, Wiley. P. 8, 27-28
[4] Gabriel Vasilescu , *Electronic noise and interfering signals: principles and applications.* P. 61
[5] Gary Davis, Ralph Jones, *The sound reinforcement handbook* Yamaha, 1988. Pg 82-85
[6] Analog Devices. *Op Amp Application Handbook.* Newnes, 2005.